Journal of Computational Physics 228 (2009) 6479–6495

Contents lists available at ScienceDirect

Journal of Computational Physics

journal homepage: www.elsevier.com/locate/jcp

Optimal preconditioning of lattice Boltzmann methods

Salvador Izquierdo, Norberto Fueyo *

Fluid Mechanics Group (University of Zaragoza) and LITEC (CSIC), María de Luna 3, 50018 Zaragoza, Spain

ARTICLE INFO

Article history:
Received 20 January 2009
Received in revised form 19 May 2009
Accepted 27 May 2009
Available online 6 June 2009

Keywords:
Lattice Boltzmann
Multi-relaxation-times
Preconditioning
Linear-stability analysis
Acceleration of convergence
Steady state
Microflow
Smoother

ABSTRACT

A preconditioning technique to accelerate the simulation of steady-state problems using the single-relaxation-time (SRT) lattice Boltzmann (LB) method was first proposed by Guo et al. [Z. Guo, T. Zhao, Y. Shi, Preconditioned lattice-Boltzmann method for steady flows, Phys. Rev. E 70 (2004) 066706-1]. The key idea in this preconditioner is to modify the equilibrium distribution function in such a way that, by means of a Chapman–Enskog expansion, a time-derivative preconditioner of the Navier–Stokes (NS) equations is obtained. In the present contribution, the optimal values for the free parameter γ of this preconditioner are searched both numerically and theoretically; the later with the aid of linear-stability analysis and with the condition number of the system of NS equations. The influence of the collision operator, single- versus multiple-relaxation-times (MRT), is also studied. Three steady-state laminar test cases are used for validation, namely: the two-dimensional lid-driven cavity, a two-dimensional microchannel and the three-dimensional backward-facing step. Finally, guidelines are suggested for an *a priori* definition of optimal preconditioning parameters as a function of the Reynolds and Mach numbers. The new optimally preconditioned MRT method derived is shown to improve, simultaneously, the rate of convergence, the stability and the accuracy of the lattice Boltzmann simulations, when compared to the non-preconditioned methods and to the optimally preconditioned SRT one. Additionally, direct time-derivative preconditioning of the LB equation is also studied.

1. Introduction

Lattice Boltzmann (LB) methods [1–5] encompass those schemes developed to solve the Boltzmann equation restricted to a finite (and minimal) number of microscopic velocities which fulfill some lattice-symmetry properties, preserving spatial invariance up to a specified order and allowing the conservation of some defined macroscopic moments (e.g. mass and momentum) [6,7]. The standard lattice Boltzmann method [8] is an explicit-time-step solver for isothermal compressible flows within the continuum and incompressible limit. It splits each temporal step in a propagation step, which accounts for advection, and in a collision step, to represent inter-particle interactions.

Due to the poor computational performance of the standard explicit collision–propagation algorithm for steady-state computations, many different approaches to accelerate lattice Boltzmann simulations have been described in the literature. To provide an overview of these techniques, first the methods to solve the discrete Boltzmann equation (DBE) are divided in lattice and non-lattice methods. Within lattice methods, only those based on the explicit collision–propagation algorithm (which is the approach used in this paper) are considered. The approaches for the acceleration of this scheme may be classified into three groups, viz.: (i) body force approaches, first proposed in [9], which apply a body force at each lattice node, proportional to the temporal variation of momentum, to accelerate the convergence to the steady state; (ii) preconditioning

* Corresponding author. Tel.: +34 976762153; fax: +34 976761882.
E-mail addresses: Salvador.Izquierdo@unizar.es (S. Izquierdo), Norberto.Fueyo@unizar.es (N. Fueyo).

0021-9991/$ - see front matter © 2009 Elsevier Inc. All rights reserved.
doi:10.1016/j.jcp.2009.05.040

of the recovered Navier–Stokes equations [10], relating the preconditioning techniques applied in Computational Fluid Dynamics to lattice Boltzmann methods; and (iii) grid-based techniques, such as multi-block [11,12], grid refinement [13] or multigrid [14,15], among others, which exploit different concepts related to the grid construction and resolution to reduce the time and memory usage needed for a specific simulation. Notice here that these techniques are conditioned by the space–time coupling existing in lattice Boltzmann methods.

A method for the acceleration of lattice Boltzmann steady-state computations should have the following desirable properties: (a) ideal acceleration ratio, which implies a linear relation between acceleration and resolution; (b) generalized formulation, so that it can be applied to all flow conditions and to any lattice Boltzmann method; (c) preservation of the collision–propagation algorithm, which confers some of the most appealing properties to the LB approach for fluid flow simulations (e.g. local computation of the collision); (d) simplicity in its implementation, because among two techniques with similar properties the simplest one will be preferentially adopted; and (e) flexibility to be combined with other acceleration or stabilization techniques, or to be ported to variable time-step and/or non-lattice schemes.

Existing acceleration techniques for the collision–propagation lattice Boltzmann scheme do not fulfill every one of these ideal conditions. Body force approaches present some problems for their generalization to recirculating or to complex-flow configurations; they also provide acceleration ratios which are far from the ideal ones. Grid-related techniques are based on quite different principles. For example, multi-block and grid-refinement methods save time by adapting the resolution of the grid only where it is necessary, their acceleration rate depends on the flow configuration, and a trade-off between computing time and accuracy can be reached. Multigrid techniques applied to lattice Boltzmann are promising but, as it is the case in traditional CFD techniques, problems in the prolongation and restriction steps near complex walls have not yet been fully addressed. Finally, preconditioning emerges as a well balanced approach to fulfill most of the ideal properties, its major drawback being the lack of knowledge about its actual stability limits and about the acceleration potential.

Preconditioning is defined, in a general sense, as the change, or conditioning, of the eigenvalues of a system of equations in order to obtain an improvement in its behavior. Therefore, preconditioning can adopt different meanings depending on the system considered or on the improvement desired. In the case of lattice Boltzmann simulations of fluid flow, a definition of preconditioning is needed to avoid ambiguity. Indeed, three different cases of preconditioning are analyzed in this work: (i) time-derivative preconditioning of Navier–Stokes equations for fluid flow acceleration and its correct asymptotic recovering of the incompressible solution; this is the classical application in CFD, and is applied in lattice Boltzmann methods through a modification of the equilibrium distribution function; (ii) time-derivative preconditioning of the lattice Boltzmann equation, which is compared in this work to under-relaxed schemes; and (iii) the multi-relaxation-times collision operator, which can be seen as a preconditioning of the collision operator in order to improve the stability of the system.

The use of time-derivative preconditioners in CFD was initially applied to compressible non-viscous flows [16]; the works by Turkel [17] and by Choi and Merkle [18] extended its application to viscous-flow solvers. In the case of viscous flows it becomes essential for compressible, low-Mach-number flows, as those addressed in many lattice Boltzmann simulations. At this low-compressibility limit, the stiffness arises from the disparity between the mean velocity of the flow and the speed of sound. The review by Turkel [19] presents a comprehensive insight into this technique. (In classical CFD, preconditioning is also applied when solving the linear problem in implicit methods; but this is a different use of preconditioning from the one studied in this work.)

Relevant previous work about preconditioners for the lattice Boltzmann equation include: the first proposal of the link between the modified equilibrium distribution function and the time-derivative preconditioner used in Navier–Stokes equations [10]; the generalization and extension to MRT [20]; and the detailed analysis of preconditioning of the lattice Boltzmann equation with a forcing term [21]. In the former work [10] a modification of the quadratic terms u^2 of the equilibrium distribution functions is proposed (γ-preconditioner). A brief stability analysis is performed and the acceleration to the steady state is verified. In [20] a new preconditioner based on the modification of the linear terms u of the equilibrium distribution function (β-preconditioner) is proved to improve γ-preconditioning results at very low-Mach numbers ($Ma < 0.05$). Additionally the method is extended to the generalized MRT collision operator, and a theoretical analysis is performed based on the condition number of the Navier–Stokes system recovered from the lattice Boltzmann equation. In the latter work [21], the γ-preconditioned MRT method is extended by considering a generalized form of the forcing term, and the method developed is applied to the simulation of a magnetohydrodynamic flow which involves the solution of a system of coupled lattice Boltzmann equations.

The main objective of the present paper is to provide theoretical and numerical results which allow to define the optimal use of the γ-preconditioner [10]. We select the γ-preconditioner due to its efficiency and simplicity: it works as well as the β-preconditioner [20] for most of the Mach numbers and, most importantly, the implementation of boundary conditions is simpler as it does not involve the rescaling of the u-terms. For the sake of simplicity, the study performed is for the two-dimensional $D2Q9$, but it can be straightforwardly extended to other lattices.

The paper is organized as follows: first, in Section 2, a description is given of the preconditioned lattice Boltzmann method with the multi-relaxation-time collision operator and the recovered Navier–Stokes equations. In Section 3, results are shown for the linear-stability analysis of the Navier–Stokes-based preconditioning of the lattice Boltzmann equation. This linear-stability analysis serves as a guide in the selection of optimal preconditioning parameters. Sections 4–6 present and discuss the results for the test cases, both 2D (lid-driven cavity and a microchannel) and 3D (backward-facing step). Finally, the conclusions of the work, suggestions for further improvements of the method and possible extensions are presented.

2. Lattice Boltzmann method with preconditioning

The lattice Boltzmann equation can be derived from the Boltzmann one [7,6], which is an equation for the evolution of the particle–velocity distribution, by discretizing the velocity space using a finite set of velocity vectors:

$$\frac{\partial \mathbf{f}}{\partial t} + \mathbf{e}_i \frac{\partial}{\partial x_i}\mathbf{f} = \mathbf{\Omega}; \tag{1}$$

where $\mathbf{f}$ is the particle distribution function, $\mathbf{e}_i$ is the discrete set of velocities and $\mathbf{\Omega}$ is the collision operator. A particular scheme is obtained by using an Euler time discretization and an upwind spatial one:

$$\mathbf{f}(x_i + \mathbf{e}_i\delta t, t+\delta t) - \mathbf{f}(x_i + \mathbf{e}_i\delta t, t) + \frac{\mathbf{e}_i\delta t}{\delta x}\mathbf{f}(x_i + \mathbf{e}_i\delta t, t) - \mathbf{f}(x_i, t) = \mathbf{\Omega}(x_i, t); \tag{2}$$

where, when $(\mathbf{e}_i\delta t)/\delta x = 1$, then $CFL = 1$. In the classical LB method, the discrete temporal and spatial steps are unity ($\delta t = 1$ and $\delta x = 1$), and they determine the lattice units. Therefore, the second and the third terms cancel each other out and it is possible to split the collision and the propagation steps as shown below.

2.1. Preconditioned multi-relaxation-time lattice Boltzmann method

A multi-relaxation-time (MRT) collision operator [22,23] is used in this work. With the usual terminology in lattice Boltzmann methods, a *DdQq* model features d dimensions and q velocities. The velocity set is $\{\mathbf{e}_i \equiv e_{i\alpha} \in V\}$ with $V = \mathbb{R}^q | \alpha = 0, 1, \ldots, N$ and $N = q - 1$. Then, a set of velocity distribution functions $\{\mathbf{f} \equiv f_\alpha \in V = \mathbb{R}^q | \alpha = 0, 1, \ldots, N\}$ is defined at each node $\{x_i \in \delta x \mathbb{Z}_d | i = 1, \ldots, d\}$. The MRT-LB evolution equation for $\mathbf{f}$, at discrete time $t \in \delta t\mathbb{N}$, is the following:

$$\mathbf{f}(x_i + \mathbf{e}_i\delta t, t+\delta t) - \mathbf{f}(x_i, t) = -\mathbf{M}^{-1}\cdot\mathbf{S}\cdot[\mathbf{m}(x_i, t) - \mathbf{m}^{eq}(x_i, t)]; \tag{3}$$

where $\mathbf{S}$ is a $q \times q$ diagonal relaxation matrix; and $\mathbf{M}$ is a $q \times q$ matrix which linearly transforms the velocity distribution functions $\mathbf{f}$ to the macroscopic moments: $\mathbf{m} = \mathbf{M}\cdot\mathbf{f}$. Equivalently, this transformation applies also for the equilibrium quantities of the macroscopic moments and of the velocity distribution functions: $\mathbf{m}^{eq} = \mathbf{M}\cdot\mathbf{f}^{eq}$. The right-hand-side of Eq. (3) results from considering the collision operator as a relaxation of the velocity distribution function toward the equilibrium (the BGK collision operator), and transforming these velocity distribution functions in their equivalent moments.

To solve the evolution equation for the particle distribution function, Eq. (3), two steps are performed:

$$\text{collision}: \quad \tilde{\mathbf{f}}(x_i, t) = \mathbf{f}(x_i, t) - \mathbf{M}^{-1}\cdot\mathbf{S}\cdot[\mathbf{m}(x_i, t) - \mathbf{m}^{eq}(x_i, t)]; \tag{4a}$$

$$\text{propagation}: \quad \mathbf{f}(x_i + \mathbf{e}_i\delta t, t+\delta t) = \tilde{\mathbf{f}}(x_i, t). \tag{4b}$$

where $\tilde{\mathbf{f}}$ represents the post-collision state.

Two lattice models are used in this paper: the $D2Q9$ and $D3Q19$ models. For simplicity, the following description applies to the two-dimensional case ($D2Q9$). The details of the $D3Q19$ model can be found in [24].

The set of velocities for $D2Q9$ are: $\mathbf{e}_x^{D2Q9} = (0, 1, 0, -1, 0, 1, -1, -1, 1)$ and $\mathbf{e}_y^{D2Q9} = (0, 0, 1, 0, -1, 1, 1, -1, -1)$. Moments for this model are: $\mathbf{m} = (\rho, e, \epsilon, j_x, q_x, j_y, q_y, p_{xx}, p_{xy})^{\mathrm{T}}$. The only macroscopic conserved variables of the flow field are density, $\rho = \rho_0 + \delta\rho$, and momentum, $(j_x, j_y) = (\rho_0 u, \rho_0 v)$, which are obtained by integrating the distribution function $\mathbf{f}$ over the velocity space: $\rho = \sum_\alpha f_\alpha = \sum_\alpha f_\alpha^{eq}$; and $\rho_0 u_i = \sum_\alpha e_{i\alpha} f_\alpha = \sum_\alpha e_{i\alpha} f_\alpha^{eq}$, where ρ_0 is a constant density, and $\delta\rho$ the density variation. As a general rule, moments are computed as $m_{ab} = \sum_\alpha (a e_{i\alpha})(b e_{i\alpha}) f_\alpha$, where $a,\ b = 0, 1, 2$. Thus, for example, $m_{00} = \rho,\ m_{10} = \rho_0 u_x$ and $m_{01} = \rho_0 u_y$. Starting from the $D2Q9$ lattice there are only nine possible linearly independent moments because the lattice itself dictates the closure for the moment equations.

The relaxation matrix for the $D2Q9$ is: $\mathbf{S} = diag(0, s_e, s_\epsilon, 0, s_q, 0, s_q, s_\nu, s_\nu)$; and the transformation matrix is:

$$\mathbf{M} = \begin{pmatrix} 1 & 1 & 1 & 1 & 1 & 1 & 1 & 1 & 1 \\ -4 & -1 & -1 & -1 & -1 & 2 & 2 & 2 & 2 \\ 4 & -2 & -2 & -2 & -2 & 1 & 1 & 1 & 1 \\ 0 & 1 & 0 & -1 & 0 & 1 & -1 & -1 & 1 \\ 0 & -2 & 0 & 2 & 0 & 1 & -1 & -1 & 1 \\ 0 & 0 & 1 & 0 & -1 & 1 & 1 & -1 & -1 \\ 0 & 0 & -2 & 0 & 2 & 1 & 1 & -1 & -1 \\ 0 & 1 & -1 & 1 & -1 & 0 & 0 & 0 & 0 \\ 0 & 0 & 0 & 0 & 0 & 1 & -1 & 1 & -1 \end{pmatrix}. \tag{5}$$

The equilibrium moments $\mathbf{m}^{eq}$ for non-conserved quantities are the following:

$$e^{eq} = -2\rho + \frac{3\rho_0(u^2 + v^2)}{\gamma}, \tag{6a}$$

$$\epsilon^{eq} = \rho - \frac{3\rho_0(u^2+v^2)}{\gamma}, \tag{6b}$$

$$q_x^{eq} = -\rho_0 u, \tag{6c}$$

$$q_y^{eq} = -\rho_0 v, \tag{6d}$$

$$p_{xx}^{eq} = \frac{\rho_0(u^2-v^2)}{\gamma} \quad \text{and} \tag{6e}$$

$$p_{xy}^{eq} = \frac{\rho_0 uv}{\gamma}. \tag{6f}$$

where we have introduced a new parameter, γ, whose role as a preconditioning parameter in the Navier–Stokes equations will be shown below. γ must be greater than 0 from stability criteria (see Section 3); and, for $\gamma = 1$, the standard lattice Boltzmann MRT method [23] is recovered, as are the original Navier–Stokes equations

The equilibrium distribution functions $f_\alpha^{eq} = M_{\alpha\beta}^{-1} m_\alpha^{eq}$ equivalent to the previous equilibrium moments have the form:

$$f_\alpha^{eq} = w_\alpha \left\{ \rho + \rho_0 \left[\frac{1}{c_s^2}(\mathbf{e}_\alpha \cdot \mathbf{u}) + \frac{1}{\gamma}\frac{1}{2c_s^4}\left((\mathbf{e}_\alpha \cdot \mathbf{u})^2 - c_s^2 \mathbf{u}\cdot\mathbf{u} \right) \right] \right\}, \tag{7}$$

where $c_s = 1/\sqrt{3}$ is the sound speed (in the $D2Q9$ and $D3Q19$ models) and weighting factors w_α are: $w_0 = 4/9,\ w_{1-4} = 1/9$ and $w_{5-8} = 1/36$. Both Eqs. (6) and (7) assume the so called 'incompressible' approximation [25], where the density is split as $\rho = \rho_0 + \delta\rho$ and the $\delta\rho u_i$ and $\delta\rho u_i^2$ terms are neglected. For $\gamma = 1$ the expression of f_α^{eq} is derived from a Taylor series expansion of the Maxwell–Boltzmann equilibrium distribution function.

By selecting the same value for all relaxation parameters in Eq. (3): $s_e = s_\epsilon = s_q = s_\nu = 1/\tau_p$, the single-relaxation-time (SRT) evolution equation is recovered:

$$\mathbf{f}(x_i + \mathbf{e}_i\delta t, t+\delta t) - \mathbf{f}(x_i,t) = -\frac{1}{\tau_p}[\mathbf{f}(x_i,t) - \mathbf{f}^{eq}(x_i,t)]; \tag{8}$$

where, now, τ_p is the only relaxation factor. The preconditioning parameter γ relates the standard and the preconditioning relaxation parameter in the following way:

$$\gamma = \frac{\tau_s - 1/2}{\tau_p - 1/2}; \tag{9}$$

where τ_s is the relaxation factor of the standard SRT lattice Boltzmann method. For $\gamma = 1$, when no preconditioning is performed, $\tau_p = \tau_s$.

2.2. Equivalent Navier–Stokes equations

Employing the Chapman–Enskog procedure [26] an expansion in terms of the Knudsen (Kn) and the Mach (Ma) numbers is performed. It is applied to Eq. (1) with the MRT collision operator and the equilibrium moments Eq. (6). For the continuum and incompressible limit (low Kn and Ma), the continuity and momentum equations are recovered:

$$\frac{\partial \rho}{\partial t} + \nabla\cdot(\rho_0 \mathbf{u}) = 0 \tag{10a}$$

$$\beta\frac{\partial(\rho_0\mathbf{u})}{\partial t} + \gamma\nabla\cdot(\rho_0\mathbf{u}\mathbf{u}) = -\nabla p + \nabla\cdot(\rho_0 \nu \mathbf{S}). \tag{10b}$$

These equations are a modification of the Navier–Stokes equations that, for convenience, we expressed in vector form:

$$\mathbf{P}_c\frac{\partial \mathbf{U}_c}{\partial t} + \frac{\partial \mathbf{E}}{\partial \mathbf{U}_c}\frac{\partial \mathbf{U}_c}{\partial x} + \frac{\partial \mathbf{F}}{\partial \mathbf{U}_c}\frac{\partial \mathbf{U}_c}{\partial y} = \frac{\partial \mathbf{E}_v}{\partial x} + \frac{\partial \mathbf{F}_v}{\partial y}. \tag{11}$$

where $\mathbf{P}_c$ is the preconditioning matrix, $\mathbf{U}_c$ are the conserved variables, $\mathbf{U}_v$ the viscous variables; in conjunction with $\mathbf{E}$, $\mathbf{F}$, $\mathbf{E}_v$ and $\mathbf{F}_v$, they are defined as:

$$\mathbf{U}_c = (\rho, \rho_0 u, \rho_0 v)^\mathsf{T}; \tag{12a}$$

$$\mathbf{U}_v = (p, u, v)^\mathsf{T}; \tag{12b}$$

$$\mathbf{E} = (\rho_0 u, \rho_0 v^2 + p, \rho_0 uv)^\mathsf{T}; \tag{12c}$$

$$\mathbf{F} = (\rho_0 v, \rho_0 uv, \rho_0 v^2 + p)^\mathsf{T}; \tag{12d}$$

$$\mathbf{E}_v = (0, \tau_{xx}, \tau_{xy})^\mathsf{T} \quad \text{and} \tag{12e}$$

$$\mathbf{F}_v = (0, \tau_{yx}, \tau_{yy})^\mathsf{T}; \tag{12f}$$

τ_{ij} being the stress tensor. The resulting preconditioned matrix in viscous variables is:

$$\mathbf{P}_v = \frac{\partial \mathbf{U}_c}{\partial \mathbf{U}_v}\mathbf{P}_c = \begin{pmatrix} 3 & 0 & 0 \\ 3u & \rho_0\gamma & 0 \\ 3v & 0 & \rho_0\gamma \end{pmatrix}. \tag{13}$$

This set of equations is closed by the state equation, in this case a modified equation for a perfect gas obtained from the Chapman–Enskog expansion, $p^* = \rho c_s^{*2}$, with a speed of sound $c_s^* = \sqrt{\gamma/3}$. The kinematic viscosity of the flow is related to the preconditioned relaxation coefficient, $s_v = 1/\tau_p$, by the equation $v = \gamma/3(1/s_v - 1/2)\delta t$. From Eq. (9):

$$s_v = \frac{1}{\tau_p} = \frac{1}{\gamma^{-1}(\tau_s - 1/2) + 1/2}. \tag{14}$$

In Eq. (14) τ_s is computed from the definition of the Reynolds number:

$$Re = \frac{u_0 N}{v} = \frac{3MaN}{\sqrt{3}(\tau_s - 1/2)}; \tag{15}$$

where $Ma = u_0/c_s$ is the Mach number, N is the number of lattice points in the characteristic length and u_0 is the reference velocity of the flow.

Due to compressibility, a bulk viscosity of the flow appears, which is defined by the s_e relaxation parameter: $\mu_B = 1/6(1/s_e - 1/2)$. For simulations performed in this work, if no other value is specified, we select the following relaxation coefficients: $s_e = s_\epsilon = 1.0$.

To study the advantages introduced by the preconditioning, an analysis of the eigenvalues of the $\mathbf{\Gamma}$ matrices can be performed [20]. These matrices are defined from Eq. (11), and are:

$$\mathbf{\Gamma}_x = \mathbf{P}_c^{-1}\frac{\partial \mathbf{E}}{\partial \mathbf{U}_c}; \tag{16}$$

and similarly for $\mathbf{\Gamma}_y$. The basic aim of preconditioning is to scale the eigenvalues of $\mathbf{\Gamma}$ appropriately, in order to reduce the stiffness of the system. To quantify the stiffness reduction the condition number (CN) is used:

$$CN = max\left(\frac{\lambda_i(\mathbf{\Gamma})}{\lambda_j(\mathbf{\Gamma})}\right); \tag{17}$$

where λ_i and λ_j are two different eigenvalues of $\mathbf{\Gamma}$. A CN close to 1 means a well balanced system with no stiffness.

The eigenvalues of $\mathbf{\Gamma}_x$ are:

$$\lambda_x = \gamma^{-1}\left(u, u/2 \pm \sqrt{(u/2)^2 + \gamma/3}\right). \tag{18}$$

Therefore, the condition number depends on the preconditioning parameter γ and on u. Considering the definition of Mach number $Ma = u/c_s$, Eq. (17) can be approximated for eigenvalues in Eq. (18), in the range $0 < \gamma < \infty$ and $Ma < \sqrt{\gamma/2}$, by:

$$CN = \frac{1}{2} + \sqrt{\frac{1}{4} + \frac{\gamma}{Ma^2}}. \tag{19}$$

To obtain $CN \to 1$, $Ma \to \infty$ or $\gamma \to 0$ is needed. $Ma > 0.3$ is not possible due to incompressibility restrictions; therefore, we study the lowest possible values for γ.

3. Linear-stability analysis

The linear-stability, or von Neumann, analysis is a standard tool to study the stability of linear and linearized systems, and has been used previously to study the stability of lattice Boltzmann methods [27], and to optimally construct new lattice Boltzmann models [23]. Additionally, it has been used as supplementary tool within the design of preconditioners for both Euler and Navier–Stokes systems of equations [18,19]. In this section we apply this technique to the selection of optimal parameters for preconditioned lattice Boltzmann schemes.

It is well known that all lattice Boltzmann models have stability limits [27]. The general stability behavior is as follows: (i) the relaxation time τ_s (with the SRT collision operator) must be grater than one-half; (ii) the mean flow speed must be smaller than a maximum stable one that is function of the other parameters; and (iii) as τ_s increases from one-half, the maximum stable speed increases monotonically until a limit is reached. Often, the high Reynolds numbers encountered in real applications bring the method close to its stability limits, viz., a relaxation factor very close to one-half and mean speed greater than the maximum stable one.

To perform the von Neumann linearized stability analysis we restrict ourselves to a steady flow, in two dimensions, with constant density ($\rho_0 = 1$), velocity $\mathbf{u}_0 = (u_0, 0)$ and wave numbers $\mathbf{k} = (k_x, 0)$ parallel to the constant velocity $\mathbf{u}_0$. These settings provide the worst stability conditions [27] (see [28] for further discussion).

The distribution function may be expressed as its equilibrium value and a small superimposed fluctuation:

$$\mathbf{f}(x_i,t) = \mathbf{f}^{eq} + \delta\mathbf{f}(x_i,t). \tag{20}$$

This formulation implies that $\mathbf{f}^{eq}$ have constant values, which do vary neither in space nor in time, and depend only on ρ_0 and u_0. The fluctuating quantities $\delta\mathbf{f}(x_i,t)$ differ from the non-equilibrium values of $\mathbf{f}$ because the linearization around equilibrium is based on mean values.

Combining Eqs. (3) and (20) with the equilibrium moments of Eq. (6) a linearized lattice Boltzmann equation for the fluctuations is obtained:

$$\delta\mathbf{f}(x_i + \mathbf{e}_i\delta t, t+\delta t) = \delta\mathbf{f}(x_i,t) + \boldsymbol{\Omega}^{eq}\cdot\delta\mathbf{f}(x_i,t) = \delta\mathbf{f}(x_i,t) + \mathbf{M}^{-1}\cdot\mathbf{C}\cdot\mathbf{M}\cdot\delta\mathbf{f}(x_i,t). \tag{21}$$

The last term is the linearized collision operator, where $\mathbf{C}$ can be written as:

$$\mathbf{C} = \frac{(\mathbf{n}\cdot\mathbf{n})_\beta}{(\mathbf{n}\cdot\mathbf{n})_\alpha}\mathbf{G}. \tag{22}$$

Here, $\mathbf{n}$ is a row vector of $\mathbf{M}$, $\mathbf{M} = \{\mathbf{n}_0,\ldots,\mathbf{n}_{q-1}\}^\top$; and $\mathbf{G}$ is the variation of the moments due to collision. Using the collision formulation of Eq. (3), this variation can be expressed as:

$$\mathbf{G} = -\mathbf{S}\mathbf{I} + \mathbf{S}\mathbf{I}\left(\frac{\partial\mathbf{m}^{eq}}{\partial\mathbf{m}}\right)_{\alpha\beta}. \tag{23}$$

For the *D*2*Q*9 model, with preconditioning equilibrium expressions, Eq. (6), we obtain:

$$G_{\alpha\beta} = \begin{pmatrix} 0 & 0 & 0 & 0 & 0 & 0 & 0 & 0 & 0 \\ -2s_e & -s_e & 0 & 6s_e u_0/\gamma & 0 & 6s_e v_0/\gamma & 0 & 0 & 0 \\ s_\epsilon & 0 & -s_\epsilon & -6s_\epsilon u_0\gamma & 0 & -6s_\epsilon v_0/\gamma & 0 & 0 & 0 \\ 0 & 0 & 0 & 0 & 0 & 0 & 0 & 0 & 0 \\ 0 & 0 & 0 & -s_q & -s_q & 0 & 0 & 0 & 0 \\ 0 & 0 & 0 & 0 & 0 & 0 & 0 & 0 & 0 \\ 0 & 0 & 0 & 0 & 0 & -s_q & -s_q & 0 & 0 \\ 0 & 0 & 0 & 2s_v u_0/\gamma & 0 & -2s_v v_0/\gamma & 0 & -s_v & 0 \\ 0 & 0 & 0 & s_v v_0/\gamma & 0 & s_v u_0/\gamma & 0 & 0 & -s_v \end{pmatrix}. \tag{24}$$

In Fourier space, Eq. (21) can be expressed as:

$$\mathbf{A}\cdot\delta\mathbf{f}(k_i,t+1) = [\mathbf{I} + \mathbf{M}^{-1}\mathbf{C}\mathbf{M}]\cdot\delta\mathbf{f}(k_i,t), \tag{25}$$

where $\mathbf{A} = -\exp(i\mathbf{e}_i k_i)\mathbf{I}$ is the advection operator. Therefore, the evolution equation may be rewritten in this form: $\delta\mathbf{f}(k_i,t+1) = \mathbf{L}\cdot\delta\mathbf{f}(k_i,t)$, with the following expression for the linearized evolution operator:

$$\mathbf{L} = \mathbf{A}^{-1}[\mathbf{I} + \mathbf{M}^{-1}\mathbf{C}\mathbf{M}]. \tag{26}$$

The linear-stability analysis performed in this work relies on the value of the maximum moduli of the eigenvalues of the linearized evolution operator $\mathbf{L}$,

$$\lambda_{max} = \mathrm{Max.}|\mathbf{L}(k_i)|,$$

which must be less than one for the system to be stable. It has been computed numerically with *Mathematica* [29].

3.1. SRT vs. MRT preconditioning

After the work by Guo et al. [10], the general guidelines for the stability criteria of preconditioned SRT lattice Boltzmann methods are known. These are: (i) τ_p must be greater than one-half; (ii) γ must be greater than a certain value which depends on the other parameters (u_i, k_i, τ_s); and (iii) as γ increases, so does the maximum speed for a stable method.

The values λ_{max} are first analyzed for the whole range of wave numbers $k_x \in [0,\pi]$, and for $\gamma \in [0,1]$. Results for $U = (0.0577, 0)$ and $\tau_s = 0.5017$, which are equivalent to $Re_x = (u_0\delta x)/\nu = 100$ and $Ma = 0.1$, are plotted in Fig. 1 for the SRT collision operator and also for the MRT one. The SRT relaxation parameter τ_s is computed with $N = 1$; and the MRT relaxation coefficients are: $s_\nu = 1/\tau_p$ and $s_e = s_\epsilon = s_q = 1.0$. Fig. 1 displays the isocontours of λ_{max}, and the areas with $\lambda_{max} > 1$ (unstable) are shaded in light gray. A first remark is that there exists a stability limit for $\gamma(\gamma_{min})$, which is approximately the same for SRT and MRT. This γ_{min} is defined by the upper limit of the isocontour $\lambda_{max} = 1.0$; and it depends on local Reynolds number Re_x and Mach number Ma. The main difference between the SRT and MRT collision operators is that for values of γ equal to or greater than the stability limit, λ_{max} will be smaller for MRT at every wave number, which means a better stability condition.

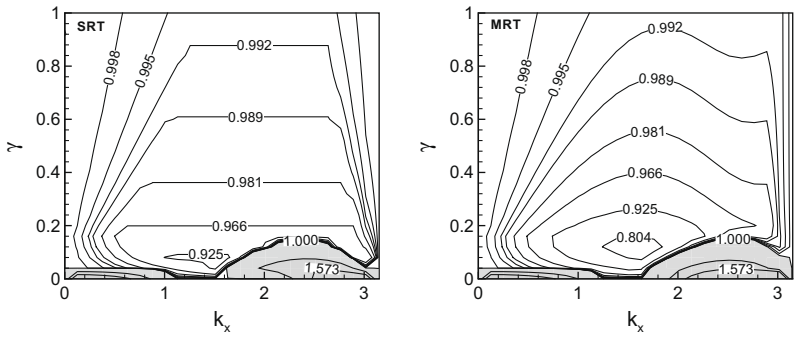

Fig. 1. Isocontours of maximum eigenvalue λ_{max} on the γ–k_x plane for the SRT (left) and MRT (right) collision operators.

3.2. Minimum values for the preconditioning parameter

To analyze the influence of the velocity u_i on the stability, λ_{max} values for different Ma and γ are plotted in Fig. 2. The value of τ_s is fixed at 0.502, and τ_p is computed as a function of γ and τ_s; the MRT relaxation parameters, other than $s_v = 1/\tau_p$, are fixed to 1.0. Results are plotted within the incompressibility limit $Ma \in [0, 0.3]$. For a given Ma number, the γ_{min} limit turns out to be approximately the same for both collision operators, but with better stability conditions for MRT. Additionally, the plots reveal that the relation between the γ_{min} limit and the Mach number is nearly linear.

Applying the stability analysis to the SRT and MRT preconditioned schemes, based on the preconditioned equilibrium distribution function, the stability criteria [10] can be redefined in the following way: (i) as $\lambda_{max} = 1 - 1/\tau_p$ in the limit when $k_i = 0$, the preconditioned relaxation parameter τ_p must be greater than one-half, or equivalently, $\tau_s > 1/2$ and $\gamma > 0$, to have a stable preconditioned lattice Boltzmann scheme; (ii) there exists a γ_{min} point close to the stability limit (Fig. 1) where the λ_{max} is the lowest, meaning grater stability, and this stability is better for MRT; (iii) there is a nearly linear relation between the γ_{min} limit and the Mach number (Fig. 2).

3.3. Optimal preconditioning parameters

To analyze a possible *a priori* selection of an optimal value for the preconditioning parameter, γ_{op}, a graphical representation of the relationship between γ, τ_s and τ_p is depicted in Fig. 3. Two superimposed relations are plotted: the first one is from the linear-stability analysis and it shows the maximum eigenvalue of $\mathbf{L}$ as a function of the preconditioning relaxation parameter τ_p and of γ; the second relationship is the one arising from Eq. (9).

While an analytical expression for γ_{op} could be useful, it is not possible to obtain one from linear-stability analysis, and only indications, based on the results, can be provided. Thus, γ_{op} may be restricted between the minimum allowable preconditioning parameter γ_{min} due to stability criteria, and the set of all points on the τ_p–γ plane where for each fixed τ_s the minimum value of λ_{max} is found. This may be expressed as:

$$\gamma_{op}(Re_x, Ma) \in \{\gamma_{min}, \gamma[\tau_s(Re_x, Ma), min.\lambda_{max}(Re_x, Ma, s_\alpha)]\}. \tag{27}$$

In preconditioned lattice Boltzmann simulations using the scheme proposed, the gain obtained can be viewed as a change from the relaxation parameter, τ_s, which determines the actual Reynolds number of the flow, to a fictitious preconditioning relaxation parameter, τ_p, which accounts for the behavior of the simulation. Thus, the larger τ_p is, the more stable and better

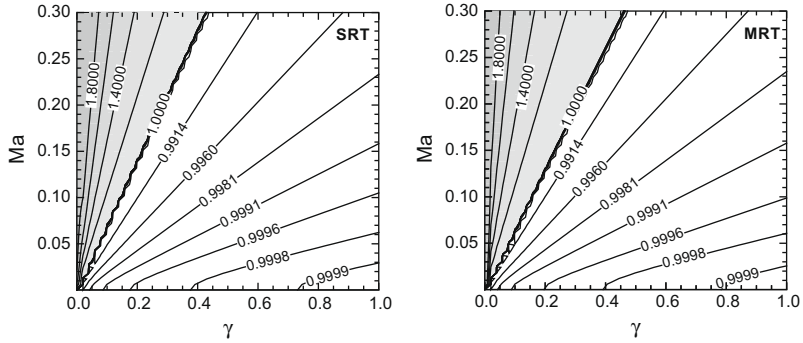

Fig. 2. Maximum eigenvalue in the whole range of k_x for different γ–Ma values for the SRT and MRT collision operators.

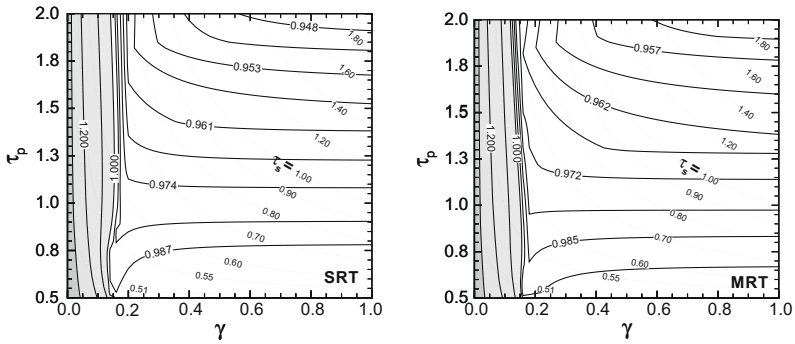

Fig. 3. Maximum eigenvalue in the whole range of k_x for different $\gamma-\tau_p$ values for the SRT and MRT collision operators. Isocontours of τ_s as a function of γ and τ_p are plotted with dotted lines.

preconditioned the system will be; however, large τ_p for a given τ_s fall beyond the stability limit. On the other hand, for large τ_s values, the optimal point could be displaced to γ values larger than γ_{min} because a compromise between large τ_p and small λ_{max} must be reached. This is the case of the microchannel analyzed in Section 5.

3.4. Global map of stability limits

In this section the limits of the MRT preconditioned scheme are explored by means of a more general stability analysis ($\gamma \in (0, \infty)$), and a study of the condition number (CN) of the recovered Navier–Stokes equation.

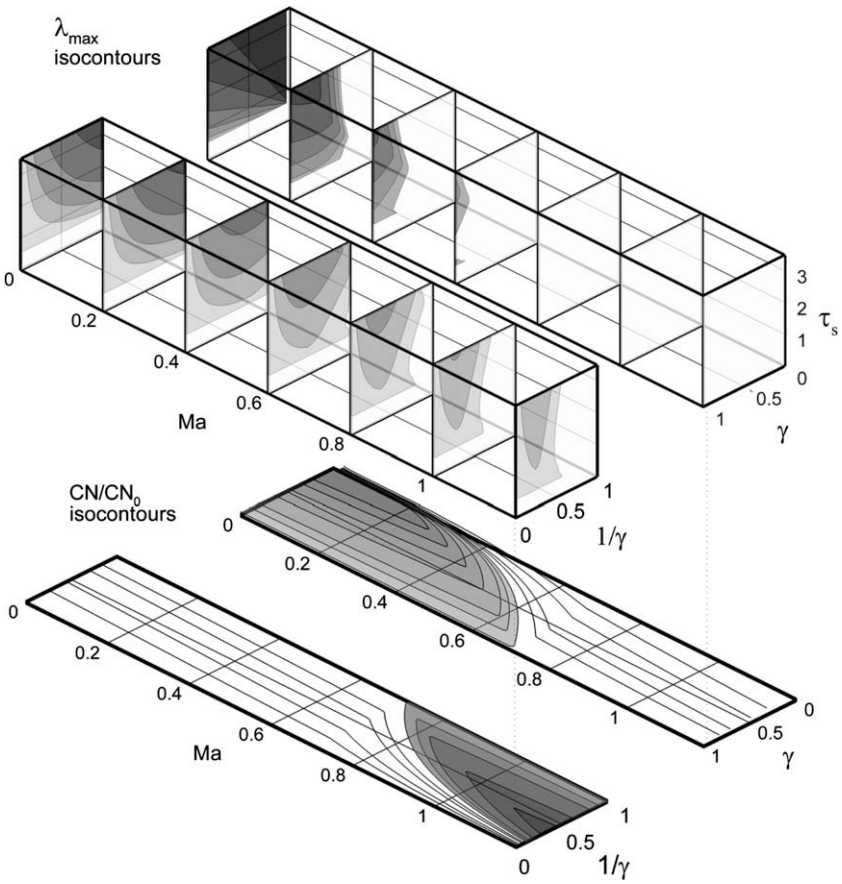

Fig. 4. (top) Global map of λ_{max} for different values of Ma and τ_s and for the whole range of γ (above). (bottom) Isocontours of the ratio between the condition number (CN) and the condition number for $\gamma = 1 (CN_0)$ for the same Ma and γ interval.

Fig. 4 summarizes the results from the analysis. First, in the top-right part of Fig. 4 we plot stability maps of τ_s vs. $\gamma \in (0,1)$ for different Mach numbers between $Ma = 0$ and $Ma = 1.2$. The analysis performed above is for the incompressible area of this part of the diagram. Isocontours of λ_{max} are plotted in a gray shade where the method is stable (darker shades indicating more stable schemes), and unstable regions are drawn in white. The main observation is that as the Mach number increases, the stable area is reduced and γ_{min} linearly increases. Additionally, for $Ma \to 0$ the stability contour becomes linear. To complement this information, the ratio between the condition number of each Ma–γ point and the condition number for this point at $\gamma = 1 (CN/CN_0)$ is plotted below the stability map. Grey areas indicate acceleration regions, and the convergence rate to the steady state is faster the darker the shade is. The zone of greater acceleration is the same as the one for γ_{min}, and therefore, stabilization and acceleration can be achieved at the same time.

On the left-hand-side of Fig. 4, the same relations are plotted for $\gamma \in (1,\infty)$. It is worth noting that the stability of the method is now greater, as it remains stable beyond $Ma = 1$; however, for the incompressible limit, the method is ill-conditioned, and no acceleration is obtained. As the flow is isothermal, the high-Ma region has no physical interest, albeit its study can assist in the development of stabilized lattice Boltzmann methods for compressible flows.

4. Two-dimensional test case I: lid-driven cavity

A lid-driven cavity flow is chosen as two-dimensional test case due to its well-researched steady-state solution [30], and to the absence of open boundaries. The present analysis focuses on three aspects: convergence rate, stability and accuracy. Additionally, the influence of the Reynolds number on the performance of the preconditioner is studied, as is the effect of the under-relaxation of **f** within the preconditioned scheme. The domain dimensions and other flow characteristics are defined below for each case. As wall boundary conditions, the half-way bounce-back scheme is used, with the momentum transfer correction of Bouzidi et al. [31] for the moving lid.

4.1. MRT vs. SRT preconditioned LBE

The performance of the MRT and SRT preconditioned methods is first compared. A detailed previous analysis of the performance of MRT and SRT in a lid-driven cavity can be found in [32]. The study of the convergence behavior is here done by monitoring the residual errors of the velocity field between each temporal step and the previous one, the residual being computed with the L_2-norm. These residuals are shown in Fig. 5 for four lattice Boltzmann schemes for the comparison of the convergence rate. As reference case the following is chosen: $Re = 1000$, $Ma = 0.1$ and an $N \times N$ domain with $N = N_x = 129$. Therefore $u_0 = 0.057735$ and $\tau_s = 0.501732$. The main conclusion from Fig. 5 is that the optimally preconditioned MRT is indeed the method which first reaches convergence to machine accuracy (after approximately 4×10^4 time steps), while SRT methods remain far from this goal after 10^5 time steps.

As a result of the algorithmic differences between the SRT and MRT methods, the smaller number of time steps required by the MRT does not necessarily imply greater efficiency than SRT. The millions of lattice nodes updated per second (MLUPS) is used as a measure to compare performance. MLUPS include the time needed to calculate the collision, the propagation and the velocity residuals. The comparison between MRT and SRT for this two-dimensional problem is shown in Fig. 6. Simulations to compare performances were carried out on an AMD Athlon 64 at 1.8 GHz and with 512 KB of cache memory. Results indicate that the SRT collision operator is approximately 4% faster on average than MRT. This is not a significant difference, therefore the comparison between SRT and MRT on the same time scale in Fig. 5 is representative of the gain in overall performance. From Fig. 6, it can be concluded that efficiencies of MRT and preconditioned MRT are similar over the entire range

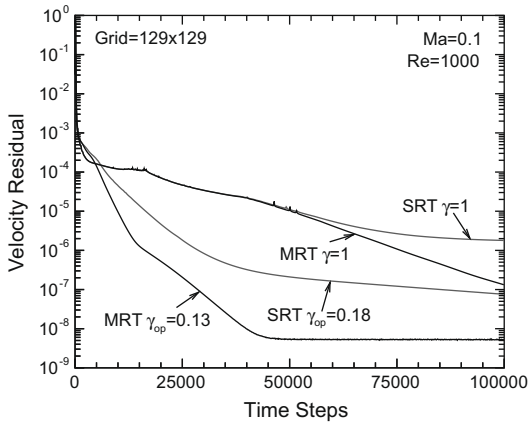

Fig. 5. Velocity residuals for the lattice Boltzmann equation with SRT and MRT, and optimal preconditioned versions of both collision operators. The values of γ used in each case are indicated.

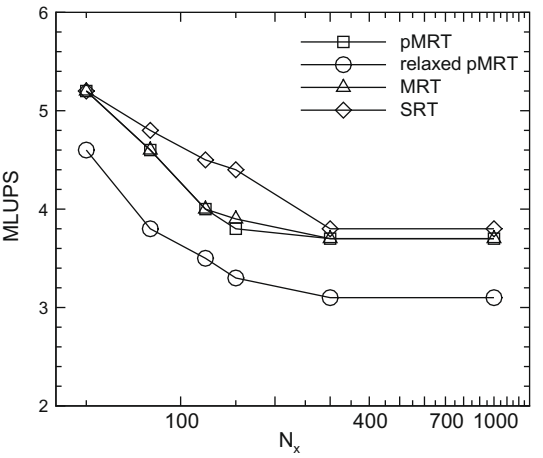

Fig. 6. Millions of lattice update per second (MLUPS) as a function of the number of cells. The total number of cells is: $N_{total} = N_x^2$.

ich indicates that the preconditioning method suggested does not add any additional significant algorithmic com-
The remaining results shown in Fig. 6 are for the under-relaxed scheme that will be discussed in Section 4.3.
ual indication of the stability improvement achieved with preconditioning is shown in the pressure contours of Fig. 7.
ther the preconditioned SRT, the MRT or the preconditioned MRT schemes results in a very significant reduction in
sure oscillations. However, with both preconditioned SRT and standard MRT some small oscillations do remain close
the cavity corners; these are completely suppressed with the preconditioned MRT scheme proposed.

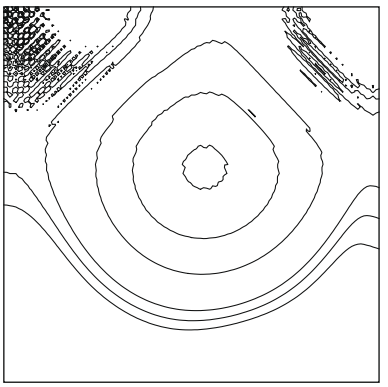

The accuracy of the results is measured against the benchmark simulations by Botella and Peyret [33]. This comparison is shown in Fig. 8. A relatively coarse lattice dimension of $N = 129$ was chosen to highlight differences in accuracy between non-preconditioned and preconditioned schemes, the latter ones providing more accurate results.

It is worth pointing that the values selected for the relaxation parameters (s_e, s_ϵ) are not optimal in the sense that they provide the maximum grade of dissipation through the bulk viscosity. The optimal values can be approximated by means of linear-stability analysis, as in [32]; however, they will be always an approximation to the optimal ones. If quasi-optimal relaxation parameters were used instead in this analysis, the conclusions could slightly vary in either directions when comparing the SRT and the MRT collision operators.

4.2. Effect of Re on the preconditioning performance

To study the effect of parameters that define the flow ($Re,\ Ma,\ N$ and s_v) on the MRT preconditioning performance, the time steps needed to reach machine accuracy are analyzed for each Reynolds number as a function of $Ma,\ N$ and τ_s. This accuracy is 5×10^{-9} for the conserved macroscopic variables ρ and u_i. Three parametric studies are performed, for the variation respectively of the number of lattice nodes, of the Ma number, and of $s_v = 1/\tau_s$. Additionally, the dependence of the optimal value of γ as a function of these parameters is also analyzed.

Fig. 9(left) displays the time needed to reach machine accuracy as the number of lattice nodes is increased (for $Ma = 0.1$ and $s_v = 1/\tau_s = 1/0.55$). This time increases with the number of nodes for both preconditioned (γ_{op}) and non-preconditioned ($\gamma = 1.0$) MRT methods, but the time is always longer for the non-preconditioned scheme and the difference increases as the dimension does. For the case of the Ma dependency, with $N = 120$ and $s_v = 1/\tau_s = 1/0.55$, Fig. 10(left), the trend is different for preconditioned and non-preconditioned schemes. The latter requires a larger Ma number to reduce the computational time, but this implies loosing accuracy due to compressibility effects. The preconditioned method reduces the calculation time as the Mach number decreases, and therefore the difference between both is maximal when $Ma \to 0$. From Fig. 11(left) it can be concluded that time needed to reach machine accuracy increases for both methods with s_v, for $Ma = 0.1$ and $N = 120$, with the preconditioning MRT providing the shortest times along the entire range.

Summarizing from these results, the best improvements with the MRT preconditioner are obtained at moderate Reynolds numbers, $\tau_s = 1/s_v = (0.53, 0.55)$, with low velocities, $Ma < 0.1$, and high-resolution meshes. With these parameters, the errors due to compressibility and discretization will also be reduced, and the problem remains well within the stability region $\tau_s > 0.5$.

The evolution of γ_{op} as a function of $N,\ Ma$ and $s_v = 1/\tau_s$ is shown on the right-hand-side plots of Figs. 9–11. The optimal value has no dependence on $s_v = 1/\tau_s$, a weak dependence on N and linear dependence on Ma. The nearly linear relation obtained from the stability analysis, Fig. 2, is plotted for comparison in Fig. 10, as well as the line $\gamma_{op} = Ma$.

4.3. Under-relaxation effect on preconditioner performance

Starting from Eq. (2), the viability of a direct time-marching preconditioning of the lattice Boltzmann equation is now studied, as an alternative to find lattice Boltzmann equations which lead to preconditioned Navier–Stokes systems. To modify this scheme, the temporal term of each equation is multiplied by a constant factor ϕ equal for all $\mathbf{f}$, which is expected to modify the convergence behavior without introducing any modification to the steady-state solution. The following modified discretization results:

$$\phi[\mathbf{f}(x_i + \mathbf{e}_i\delta t, t + \delta t) - \mathbf{f}(x_i + \mathbf{e}_i\delta t, t)] + \frac{\mathbf{e}_i\delta t}{\delta x}\mathbf{f}(x_i + \mathbf{e}_i\delta t, t) - \mathbf{f}(x_i, t) = -\delta t\mathbf{M}^{-1}\cdot\mathbf{S}\cdot[\mathbf{m}(x_i, t) - \mathbf{m}^{eq}(x_i, t)]. \tag{28}$$

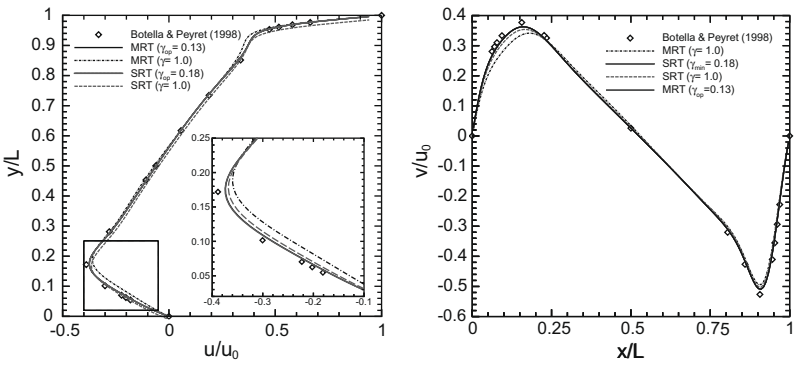

Fig. 8. Comparison with calculated reference data [33], for the same cases as in Figs. 5 and 7, of horizontal velocity component u (left), and vertical velocity component v (right).

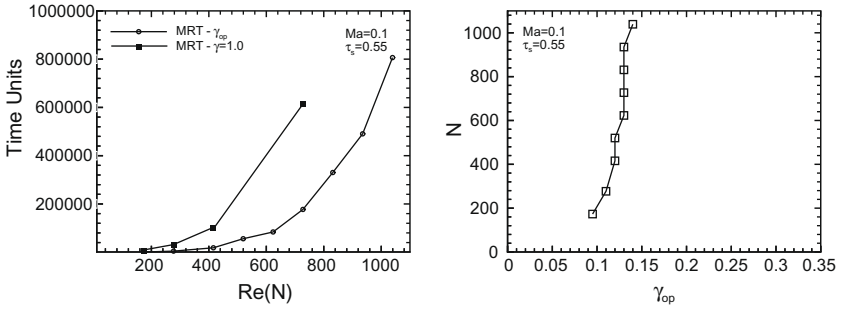

Fig. 9. (left) Time units (referred to $N = 120$ for normalization) needed to reach machine accuracy, as a function of Reynolds number which varies by changing N; (right) optimal value of the preconditioning parameter, γ_{op}, as a function of the number of cells.

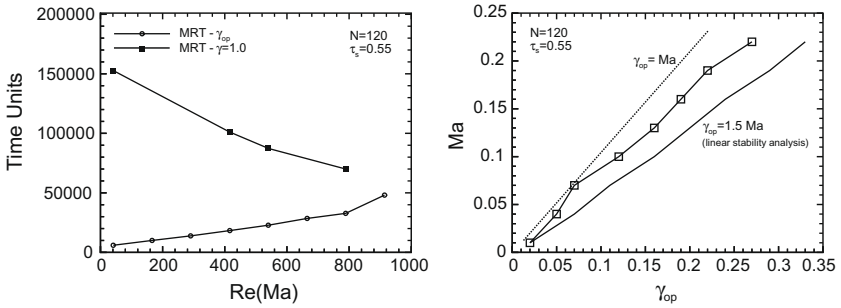

Fig. 10. (left) Time units needed to reach machine accuracy versus Reynolds number, computed as a function of Mach number; (right) optimal value of the preconditioning parameter, γ_{op}, as a function of Mach number.

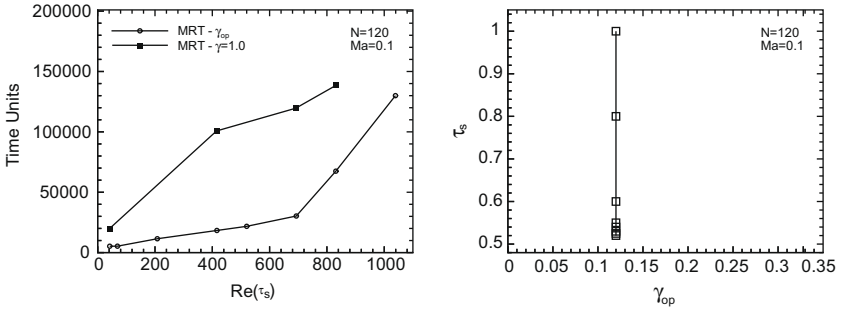

Fig. 11. Time units needed to reach machine accuracy versus Reynolds number, computed as a function of relaxation factor $s_\nu = 1/\tau_s$ (left); optimal value of the preconditioning parameter, γ_{op}, as a function of relaxation factor (right).

Simple algebraic manipulation of this equation leads to the following collision–propagation algorithm:

$$\text{collision}: \quad \tilde{\mathbf{f}}(x_i,t) = [\phi\mathbf{f}(x_i,t) + (1-\phi)\mathbf{f}(x_i,t-\delta t)]\mathbf{f}^*(x_i,t) - \mathbf{M}^{-1}\cdot\mathbf{S}\cdot[\mathbf{m}(x_i,t) - \mathbf{m}^{eq}(x_i,t)], \tag{29a}$$

$$\text{propagation}: \quad \mathbf{f}(x_i + \mathbf{e}_i\delta t, t+\delta t) = \tilde{\mathbf{f}}(x_i,t); \tag{29b}$$

where $\mathbf{f}^*(x_i,t) = \phi\mathbf{f}(x_i,t-\delta t) + (1-\phi)\mathbf{f}(x_i,t-2\delta t)$. This scheme can be viewed as a standard collision–propagation algorithm plus a temporal under-relaxation of $\mathbf{f}$ variables. It is actually a Jacobi iteration. The scheme can be improved by using other classic iterators, as the Gauss–Seidel one, but losing locality in the collision step.

An under-relaxation coefficient $\phi = 0.8$ is selected, and results for the γ-preconditioned versions of the SRT and MRT collision operators are shown in Fig. 12. In the SRT case, when adding under-relaxation to the optimal γ-preconditioning ($\gamma = 0.18$), it is possible to reach lower residual values. The under-relaxation modifies the stability behavior and, therefore it also is possible to select smaller values of γ; thus, using a newly-found optimal value of the preconditioning parameter ($\gamma = 0.11$), less time is needed to reach machine accuracy. In the case of MRT (right plot in Fig. 12), these improvements are not so obvious, and under-relaxation can even worsen convergence if the value of γ is maintained. However, a new

The velocity profile along the x direction from the lattice Boltzmann simulation is shown in Fig. 13 to illustrate the non-linear behavior of the gas flow in a microchannel. As the gas moves downstream the pressure drop increases, and so does the Knudsen number; therefore, the slip becomes larger and the mass flow increases.

In Fig. 14 the normalized velocity profiles at outlet are plotted for different Knudsen numbers, as well as the normalized pressure profiles along the channel. Results from the non-preconditioned lattice Boltzmann method differ slightly from those obtained from the preconditioned one. However, as it can be seen in Fig. 15(left) the accuracy is always better with the preconditioned lattice Boltzmann approach.

Due to the compressibility effects described above a variable viscosity is used, which serves also the purpose of validating the method for these situations. The optimal values of γ are for this reason very different from those derived from the linear-stability analysis (Fig. 15(right)). The optimal γ value is conditioned by the maximum τ_s in the domain, and for large values of τ_s, γ_{op} increases as predicted by the linear-stability analysis (Fig. 3). In this Fig. 3, for values $\tau_s > 0.8$ the region with lower λ_{max} is no longer close to the stability limit.

6. Three-dimensional test case: backward-facing step

The previous results and analysis for the $D2Q9$ model can be extended for other lattice geometries. Here, the application to the $D3Q19$ model is presented. The description of the $D3Q19$ model can be found in [24], the corresponding equilibrium moments are in Appendix A, and in this section some salient results are briefly described.

The backward-facing step is the selected test case. At wall boundaries, the half-way bounce-back condition is used; at the inlet a constant velocity (u_0) is set using [31]; and at the outlet a convective condition for $\mathbf{f}$ is applied [40]. Based on results of Armaly et al. [41] a Reynolds number equal to 100 has been chosen; therefore, the flow remains laminar. The geometry, streamlines and recirculation length for the test case are plotted in Fig. 16; and in Fig. 17 a comparison between numerical and experimental results is shown. The reattachment length is $x_r/L = 3.2$, which agrees well with the experimental value of Armaly et al. [41] $x_r/L = 3.1$.

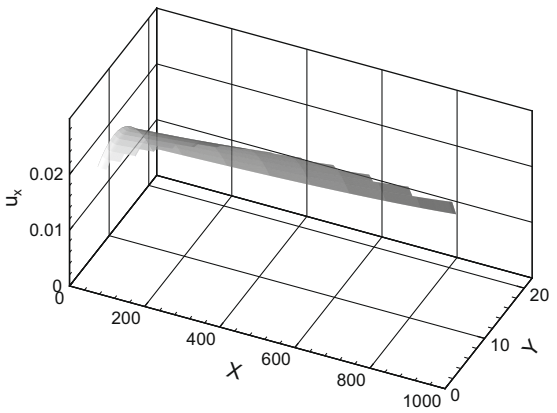

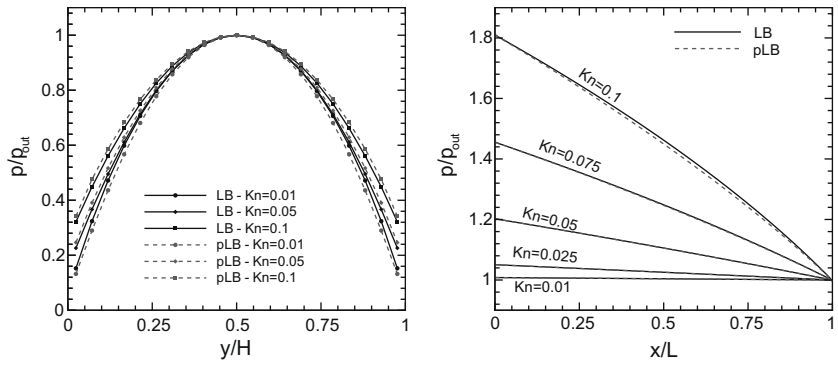

Fig. 14. Velocity (left) and pressure (right) profiles obtained for the microchannel.

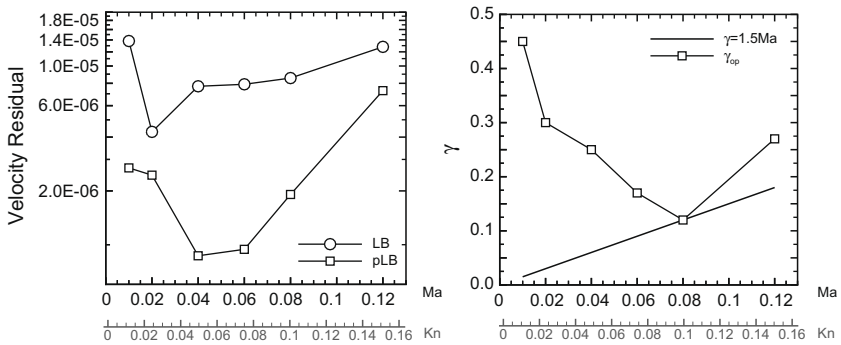

Fig. 15. Accuracy with (pLB) and without (LB) preconditioning for the microchannel (left); and optimal values for γ (right).

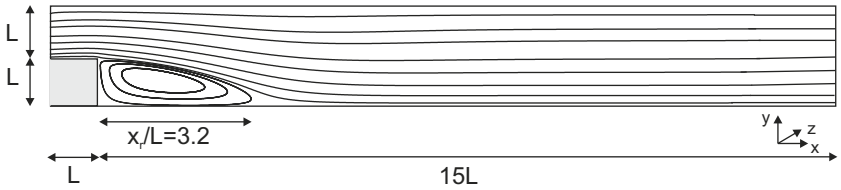

Fig. 16. Backward-facing step: domain dimensions and streamlines for $Re = 100$.

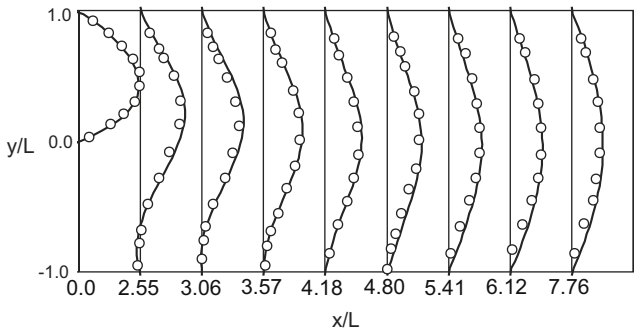

Fig. 17. Velocity profiles at different dimensionless lengths x/L (black lines); and experimental results for $Re = 100$ from Armaly et al. [41] (white dots).

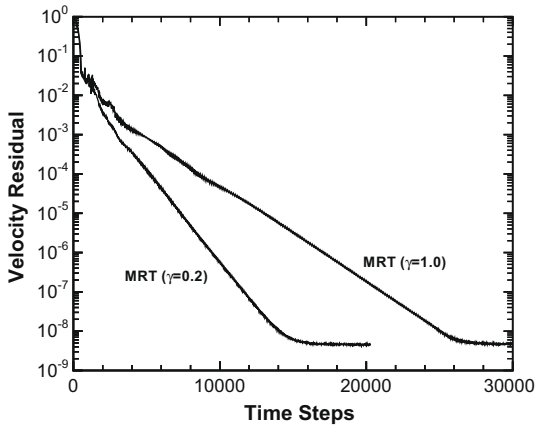

Fig. 18. Evolution of velocity residual for two MRT simulations of the backward-facing step: preconditioned ($\gamma_{op} = 0.2$) and non-preconditioned ($\gamma = 1$).

As in the two-dimensional test case, the residual evolutions are plotted, Fig. 18, to evaluate the improvement in the convergence performance. As for the $D2Q9$ model, preconditioning makes it possible to reduce the time needed to attain a target accuracy. For the $D3Q19$ lattice the optimal value for the preconditioner parameter is found numerically to be $\gamma_{op} = 2Ma$.

7. Conclusions

The stabilization of the solution of the lattice Boltzmann equation was an early [22] but nowadays very active research topic [42–44] and it seems to be paramount for the emergence of LBM as a competitive CFD technique. Additionally, acceleration is necessary for the efficient explicit computation of steady states. The optimal preconditioned lattice Boltzmann equation allows to achieve these two desired properties with an additional improvement in accuracy. In summary, the following conclusions can be derived from the work done.

Optimal equilibrium-based preconditioners for lattice Boltzmann methods defined with the aid of the Chapman–Enskog expansion, a linear-stability analysis, and the condition number of the equivalent Navier–Stokes equations, are proved to be a simple and efficient technique to accelerate steady-state computations. The main advantage is that, by switching to an MRT collision operator and adding a minor modification to the standard LB algorithm, it is possible to reduce by about an order of magnitude the computational time for steady-state simulations. This time reduction varies with the flow parameters, and could be even greater. Additionally, better accuracy and stability are obtained. The local definition of the free parameter could improve the preconditioner behavior; however this is not trivial in the standard scheme due to the spatio-temporal constraints which relate all the information within the domain.

The optimal values for γ depend on the characteristics of the flow configuration but lie in the range $\gamma_{op} = (1.0Ma, 1.5Ma)$, as obtained from linear-stability analysis and simulations for the $D2Q9$ LB method. From simulations, $\gamma_{op} = 2.0Ma$ is obtained for the $D3Q19$ method. For very low Reynolds numbers $(\tau_s > 2)$, γ_{op} increases from this values.

Direct preconditioning of the lattice Boltzmann equation can be also applied, but the attempt made in this direction indicates it is less effective than Navier–Stokes-based preconditioning. A direct time-derivative lattice Boltzmann preconditioner can be viewed as an under-relaxation which introduces no significant improvement in the behavior of preconditioned schemes proposed in this work. Results obtained point to the possibility of successfully replacing under-relaxation by theα

$$p_{yz}^{eq} = \frac{\rho_0 vw}{\gamma} \quad \text{and} \tag{35f}$$

$$p_{xz}^{eq} = \frac{\rho_0 uw}{\gamma}. \tag{35g}$$

References

[1] R. Benzi, S. Succi, M. Vergassola, The lattice Boltzmann equation: theory and applications, Phys. Rep. 222 (1992) 3.
[2] S. Chen, G. Doolen, Lattice Boltzmann method for fluid flows, Annu. Rev. Fluid Mech. 30 (1998) 329–364.
[3] D. Wolf-Gladrow, Lattice-Gas Cellular Automata and Lattice Boltzmann Models. An Introduction, Lecture Notes in Mathematics, Lecture Notes in Mathematics, vol. 1725, Springer, Berlin, 2000.
[4] S. Succi, The Lattice Boltzmann Equation for Fluid Dynamics and Beyond, Oxford, 2001.
[5] D. Yu, R. Mei, L.-S. Luo, W. Shyy, Viscous flow computations with the method of lattice Boltzmann equation, Prog. Aerosp. Sci. 39 (2003) 329–367.
[6] X. He, L.-S. Luo, Theory of lattice Boltzmann method: from the Boltzmann equation to the lattice Boltzmann equation, Phys. Rev. E 56 (1997) 6811–6817.
[7] S.S. Chikatamarla, I.V. Karlin, Entropy and Galilean invariance of lattice Boltzmann theories, Phys. Rev. Lett. 97 (2006) 190601.
[8] Y. Qian, D. d'Humières, P. Lallemand, Lattice BGK models for Navier–Stokes equation, Europhys. Lett. 17 (1992) 479–484.
[9] D. Kandhai, A. Koponen, A. Hoekstra, M. Kataja, J. Timonen, P. Sloot, Implementation aspects of 3D lattice-BGK: boundaries accuracy and a fast relaxation method, J. Comput. Phys. 150 (1999) 1–20.
[10] Z. Guo, T. Zhao, Y. Shi, Preconditioned lattice-Boltzmann method for steady flows, Phys. Rev. E 70 (2004) 066706-1.
[11] C. Lin, Y. Lai, Lattice Boltzmann method on composite grids, Phys. Rev. E 62 (2000) 2219–2225.
[12] D. Yu, R. Mei, W. Shyy, A multi-block lattice Boltzmann method for viscous fluid flow, Int. J. Numer. Method Fluid 39 (2002) 99–120.
[13] O. Filippova, D. Hänel, Acceleration of lattice-BGK schemes with grid refinement, J. Comput. Phys. 165 (2000) 407–427.
[14] J. Tölke, M. Krafczyk, E. Rank, A multigrid solver for the discrete Boltzmann equation, J. Stat. Phys. 107 (2002) 573–591.
[15] D.J. Mavriplis, Multigrid solution of the steady-state lattice Boltzmann equation, Comput. Fluid 35 (2006) 793–804.
[16] H. Viviand, Numerical Methods for the Euler Equations of Fluid Dynamics, SIAM, 1985.
[17] E. Turkel, Preconditioned methods for solving the incompressible and low-speed compressible equations, J. Comput. Phys. 72 (1987) 277–298.
[18] Y. Choi, C. Merkle, The application of preconditioning in viscous flows, J. Comput. Phys. 105 (1993) 207–223.
[19] E. Turkel, Preconditioning techniques in computational fluid dynamics, Annu. Rev. Fluid Mech. 31 (1999) 385–416.
[20] S. Izquierdo, N. Fueyo, Preconditioned Navier–Stokes schemes from the generalized lattice Boltzmann equation, Prog. Comput. Fluid Dynam. 8 (1–4) (2008) 189–196.
[21] K.N. Premnath, M.J. Pattison, S. Banerjee, Steady state convergence acceleration of the generalized lattice Boltzmann equation with forcing term through preconditioning, J. Comput. Phys. (2008), doi:10.1016/j.jcp.2008.09.028.
[22] D. d'Humières, Generalized lattice-Boltzmann equations, AIAA rarefied gas dynamics: theory and simulations, Prog. Astronaut. Aeronaut. 59 (1992) 450–548.
[23] P. Lallemand, L.-S. Luo, Theory of the lattice Boltzmann method: dispersion, dissipation, isotropy, Galilean invariance and stability, Phys. Rev. E 61 (2000) 6546–6562.
[24] J. Tölke, S. Freudiger, M. Krafczyk, An adaptive scheme using hierarchical grids for lattice Boltzmann multi-phase flow simulation, Comput. Fluid 35 (2006) 820–830.
[25] X. He, L.-S. Luo, Lattice Boltzmann model for the incompressible Navier–Stokes equation, J. Stat. Phys. 88 (1997) 927–944.
[26] S. Chapman, T. Cowling, The Mathematical Theory of Non-uniform Gases, third ed., Cambridge University Press, Berlin, 1991.
[27] J. Sterling, S. Chen, Stability analysis of lattice Boltzmann methods, J. Comput. Phys. 123 (1996) 196–206.
[28] D.N. Siebert, L.A. Hegele Jr., P.C. Philippi, Lattice Boltzmann equation linear stability analysis: thermal and athermal models, Phys. Rev. E 77 (2008) 026707.
[29] Mathematica, Wolfram Research Inc., Version 5.0 Edition, Wolfram Research Inc., Champaign, IL, 2003.
[30] P.N. Shankar, M.D. Deshpande, Fluid mechanics in the driven cavity, Annu. Rev. Fluid Mech. 32 (2000) 93–136.
[31] M. Bouzidi, M. Firdaouss, P. Lallemand, Momentum transfer of a Boltzmann-lattice fluid with boundaries, Phys. Fluid 13 (11) (2001) 3452–3459.
[32] D. d'Humières, I. Ginzburg, M. Krafczyk, P. Lallemand, L.-S. Luo, Multiple-relaxation-time lattice Boltzmann models in three-dimensions, Philos. Trans. R. Soc. Lond. 360 (2002) 437–451.
[33] O. Botella, R. Peyret, Benchmark spectral results on the lid-driven cavity flow, Comput. Fluid 27 (1998) 421–433.
[34] X. Niu, C. Shu, Y. Chew, A thermal lattice Boltzmann model with diffuse scattering boundary condition for microthermal flows, Comput. Fluid 36 (2007) 273–281.
[35] C.M. Ho, Y.C. Tai, Micro-electro-mechanical-systems (MEMS) and fluid flows, Annu. Rev. Fluid Mech. 30 (1998) 579–612.
[36] G. Karniadakis, A. Beskok, N.R. Aluru, Microflows and Nanoflows: Fundamentals and Simulation, Springer-Verlag, New York, 2005.
[37] E.B. Arkilic, M.A. Schmidt, K.S. Breuer, Gaseous slip flow in long microchannels, J. Microelectromech. Syst. 6 (2) (1997) 167–178.
[38] M. Sbragaglia, S. Succi, Analytical calculation of slip flow in lattice Boltzmann models with kinetic boundary conditions, Phys. Fluid 17 (2005) 093602.
[39] T. Lee, C.-L. Lin, Rarefaction and compressibility effects of the lattice-Boltzmann-equation method in a gas microchannel, Phys. Rev. E 71 (2005) 046706.
[40] D. Yu, R. Mei, W. Shyy, Improved treatment of the open boundary in the method of lattice Boltzmann equation, Prog. Comput. Fluid Dynam. 5 (1/2) (2005) 3–12.
[41] B. Armaly, F. Durst, J. Pereira, B. Schnung, Experimental and theoretical investigation of backward-facing step flow, J. Fluid Mech. 127 (1983) 473–496.
[42] R.A. Brownlee, A.N. Gorban, J. Levesley, Stability and stabilization of the lattice boltzmann method, Phys. Rev. E 75 (2007) 036711.
[43] M. Geier, A. Greiner, J.G. Korvink, Cascaded digital lattice Boltzmann automata for high Reynolds number flow, Phys. Rev. E 73 (6) (2006) 066705.
[44] J. Latt, B. Chopard, Lattice Boltzmann method with regularized pre-collision distribution functions, Math. Comput. Simul. 72 (2–6) (2006) 165–168.
[45] M. Junk, A. Klar, L.-S. Luo, Asymptotic analysis of the lattice Boltzmann equation, J. Comput. Phys. 210 (2005) 676–704.
[46] I. Ginzburg, F. Verhaeghe, D. d'Humières, Two-relaxation-time lattice boltzmann scheme: about parametrization, velocity, pressure and mixed boundary conditions, Commun. Comput. Phys. 3 (2) (2008) 427–478.